On eigenmodes, stiffness, and sensitivity of atomic force microscope cantilevers in air versus liquids

Daniel Kiracofe and Arvind Raman[a)]
Birck Nanotechnology Center and School of Mechanical Engineering, Purdue University, West Lafayette, Indiana 47904-2088, USA

(Received 20 August 2009; accepted 3 December 2009; published online 2 February 2010)

The effect of hydrodynamic loading on the eigenmode shapes, modal stiffnesses, and optical lever sensitivities of atomic force microscope (AFM) microcantilevers is investigated by measuring the vibrations of such microcantilevers in air and water using a scanning laser Doppler vibrometer. It is found that for rectangular tipless microcantilevers, the measured fundamental and higher eigenmodes and their equivalent stiffnesses are nearly identical in air and in water. However, for microcantilevers with a tip mass or for picket shaped cantilevers, there is a marked difference in the second (and higher) eigenmode shapes between air and water that leads to a large decrease in their modal stiffness in water as compared to air as well as a decrease in their optical lever sensitivity. These results are explained in terms of hydrodynamic interactions of microcantilevers with nonuniform mass distribution. The results clearly demonstrate that tip mass and hydrodynamic loading must be taken into account in stiffness calibration and optical lever sensitivity calibration while using higher-order eigenmodes in dynamic AFM. © *2010 American Institute of Physics*. [doi:10.1063/1.3284206]

I. INTRODUCTION AND MOTIVATION

Experimental calibration of the stiffness and optical lever sensitivity of microcantilevers is an active area of research (e.g., Refs. 1–8) due to its importance for quantitative atomic force microscopy (AFM).[9] Without accurate knowledge of the stiffness of a microcantilever and its optical lever sensitivity (photodiode output for a given tip deflection), quantitative force spectroscopy is not possible. Most AFM modes require the accurate calibration of the static bending or first eigenmode stiffness and optical lever sensitivity in order to obtain quantitative data. The experimental calibrations of the *static* bending stiffness and optical lever sensitivity are now well established techniques with quantifiable standards.[10] For the most part, the equivalent stiffness and optical lever sensitivity of the *first eigenmode* are close to those of the static values and are also well understood.[11,12]

However, there is an increasing interest in the use of higher-order eigenmodes in dynamic AFM especially for applications where small tip oscillation amplitudes are desired or where multiple eigenmodes are excited simultaneously.[13–19] Each eigenmode has an associated dynamic stiffness (also known as modal stiffness), which is different from the static stiffness. This dynamic stiffness can be related to an equivalent spring that has the same potential energy as the eigenmode.[11] Throughout this paper "stiffness" will refer to this equivalent stiffness. In contrast with the first bending eigenmode, the equivalent stiffness and optical lever sensitivity of the higher-order eigenmodes are not as well understood, especially in liquid environments. Several authors have reported difficulties calibrating the stiffness of microcantilevers in liquids.[2,20] These authors assume implicitly that stiffness is the same in air and liquid and thus suggest that it is preferable to calibrate microcantilever stiffness in air and then use that stiffness value for measurements in liquid. Additionally, in most cases only the static bending optical lever sensitivity is calibrated experimentally, and the optical lever sensitivity of the higher eigenmodes is inferred from beam theory.[6] It is usually implicitly assumed that the optical lever sensitivity of higher-order eigenmodes is the same in air and water.

In this paper, differences in hydrodynamic loading between air and liquid are investigated with the intent to determine when it is valid to use stiffness and sensitivity calibrations from air for applications in liquid and when it is not. A focus is placed on higher-order eigenmodes, in particular, on the second flexural eigenmode. Specifically, scanning laser Doppler vibrometry of AFM microcantilevers and theoretical modeling are used to explore the differences in eigenmode shapes of (a) rectangular tipless microcantilevers, (b) tipped AFM microcantilevers, and (c) picket shaped tipless microcantilevers in air and liquid. We find that the first eigenmode of such AFM microcantilevers is nearly unchanged when immersed in liquid, implying that any calibration of the first eigenmode performed in air can be used for operation in liquid. However, this common assumption can break down for the second and higher-order eigenmodes. Specifically, when the mass distribution is not perfectly uniform because of either significant tip mass (>2% of microcantilever mass) or a picket shaped end, the eigenmodes, stiffnesses, and optical lever sensitivities of the higher eigenmodes are quite different in air than in liquids. Using experiments and theory we lay out the fundamental reasons behind this interesting finding and provide theoretical estimates of the corrections that need to be made when using stiffness and optical lever sensitivities calibrated in air for application in liquid environments.

[a)]Electronic mail: raman@purdue.edu.

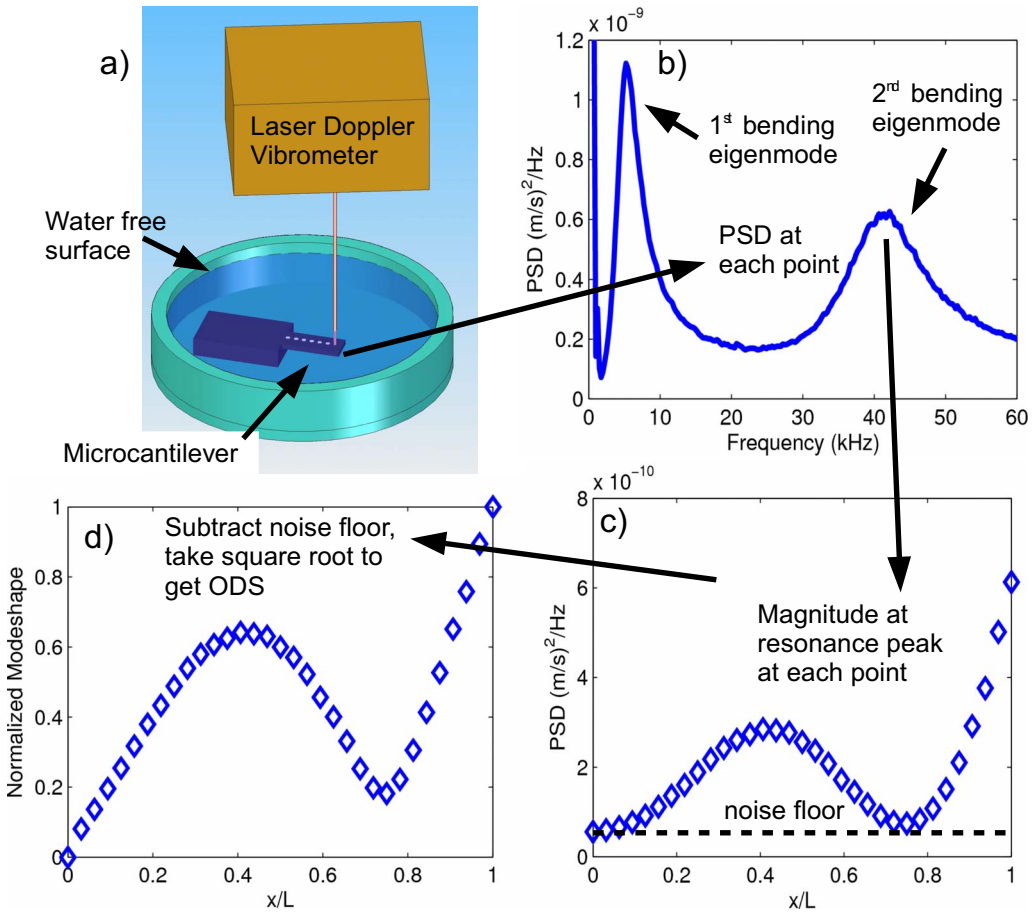

FIG. 1. (Color online) (a) Schematic of experimental setup to measure the ODSs in air and liquids. Approximately 3 s of thermal vibration data were taken per point for approximately 30 points along the axis of the microcantilever [white dots in (a)] and sampled at approximately 2.5 times the second flexural resonance frequency. (b) At each point MATLAB's pwelch command was used to estimate the PSD. For each resonance peak, the magnitude of the PSD at the corresponding points along the length was used to form a shape (c). Because the microcantilever base is stationary in this experiment, the measured thermal response signal at the base was considered to be background sensor noise and was removed from each shape. Then the square root of each point in the shape is taken to form an ODS, and the ODS is normalized so that the amplitude at the tip is unity (d).

This paper is organized as follows: First, the experimental data are presented and the results interpreted (Sec. II). Then, a theory is given that justifies the interpretation (Sec. III). The special case of picket shaped microcantilevers is discussed (Sec. IV). Finally, the results are summarized and discussed further (Sec. V).

II. EXPERIMENTS

A. Experimental method

The eigenmode shapes of various AFM microcantilevers were measured using a scanning laser Doppler vibrometer (Polytec MSA-400 Micro System Analyzer from Polytec Gmbh, Waldbronn, Germany). A schematic of the experimental setup is shown in Fig. 1. Thermally driven time series velocity data of the out-of-plane cantilever vibration were acquired in both air and water[21] at approximately 30 points along the axis of each microcantilever. From the measured power spectral density (PSD) at each point along the cantilever's length, it is possible to extract the so-called operating deflection shape (ODS) at the resonant frequencies (refer to Fig. 1 for more details).

The difference between an ODS and an eigenmode is subtle and the two are often confused. An eigenmode is the solution to the free, unforced vibration problem (homogeneous differential equation) when the system vibrates at a natural frequency. An ODS is the particular solution to a forced vibration problem (nonhomogeneous differential equation). Any ODS can be expressed as a linear combination of eigenmodes.[22] For typical AFM microcantilevers in air, because the natural frequencies are spaced far apart and the quality factors are high, each ODS is dominated by a single eigenmode, and the ODS is essentially equivalent to an eigenmode. However, in water, the quality factors are lower, therefore each ODS may contain contributions from multiple eigenmodes.[23] Specifically while the first ODS is essentially equivalent to the first eigenmode, the nth ($n \geq 2$) order ODS is a linear combination of the first n eigenmodes.

Multiple microcantilevers from different manufacturers were measured (see insets in Fig. 2); the results for five typical microcantilevers are presented. Microcantilever A is a silicon nitride beam from chip 1 of the Cantilever Array Discover Platform (Sandia National Laboratories). This microcantilever is chosen because it is perfectly rectangular and has no tip. Microcantilever B is an Olympus[24] OMCL-RC800PSA 20×200 μm^2 beam. This microcantilever was chosen because of its hollow tip, which has vanishingly small tip mass. Microcantilever C is an Agilent[25] MAC lever

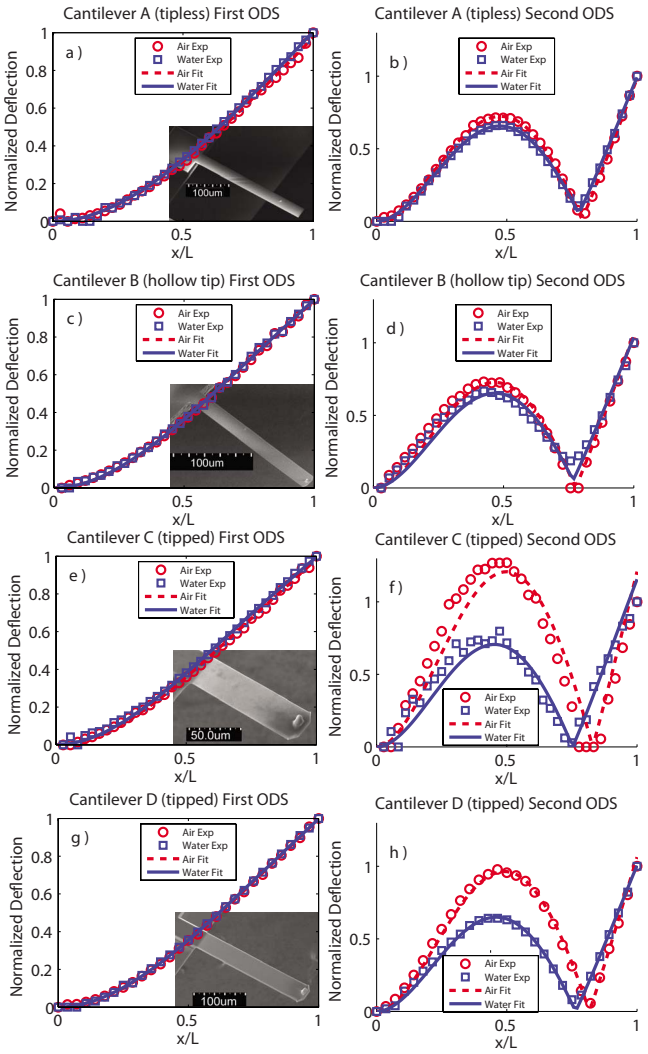

FIG. 2. (Color online) Measured ODSs for the microcantilevers in air (circles) and water (squares) and a smooth curve fit to the general eigenmode shape (see Sec. II C) in air (dashed lines) and water (solid lines). Left column first ODS (first eigenmode) and right column second ODS (first eigenmode plus second eigenmode). Because thermally driven spectra were used, phase information is not available and the absolute value of the ODS is plotted. The base of the microcantilever is to the left and the free end is to the right. Experimental data are normalized to the same displacement at the free end for all ODSs.

type I. Microcantilever D is an NSC12 lever F from Mikromasch.[26] Microcantilevers C and D were chosen because of their large, solid conical tips that add significant mass. Microcantilever E is an Applied Nanostructures[27] FORTA-TL-10. This microcantilever was chosen because it has a tipless, picket shaped end. The relevant parameters of these cantilevers are listed in Table I. Material properties of the microcantilevers and surrounding media are listed in Table II.

B. Experimental results: ODSs in air versus water

The first and second flexural ODSs from microcantilevers A (tipless), B (hollow tip), C (tipped), and D (tipped) measured in air and water are shown in Fig. 2. From this, five major conclusions can be drawn.

(1) Comparing Figs. 2(a), 2(c), 2(e), and 2(g) it is clear that the first ODS (which is approximately the first eigenmode shape) is very nearly identical in air and water for all microcantilevers tested. This means that the first eigenmode remains unchanged when a microcantilever in air is immersed in water.
(2) From Figs. 2(b) and 2(d) it is clear that the second ODS of microcantilevers A and B is approximately identical in air and water. This suggests that for cantilevers with negligible tip mass (i.e., tipless or hollow tip AFM cantilevers), the second eigenmode remains relatively unchanged when the microcantilever in air is immersed in water.
(3) However, from Figs. 2(f) and 2(h) it is clear that for cantilevers C and D, the second ODS in water is quite different from that in air. The second ODS has a significantly smaller maximum amplitude (relative to the tip) in water than in air, the node is closer to the tip in water, and the slope near the tip is steeper in water. This implies that when a microcantilever with some tip mass is immersed in water, the second eigenmode is significantly modified.
(4) In air, the second ODSs of microcantilevers A and B are similar but those of C and D are different. Microcantilever C and D's second ODS has a larger maximum amplitude than microcantilever A or B and the node is closer to the tip. This implies that in air the presence of

TABLE I. Geometric and measured parameters for the microcantilevers studied in this work.

Microcantilever	A	B	C	D	E
Manufacturer	Sandia	Olympus	Agilent	Mikromasch	Applied Nanostructures
Model	CADP 1	RC800PSA	MAC I	NSC12	FORTA-TL-10
Beam number	N/A	20×200	C	F	N/A
Material	Polysilicon	Si_3N_4	Single crystal Si	Single crystal Si	Single crystal Si
Nominal stiffness (N/m)	0.0044	0.05	0.6	0.65	3.0
Width b (μm)	29	20	35	35	25
Height h (μm)	0.5	0.8	1	2	2.5
Length L (μm)	300	200	130	250	215
Nondimensional tip mass $\frac{m_{tip}}{\rho_c AL}$	0	≈0	≈0.22	≈0.06	0
First resonance f_1 (kHz), air	33.0	19.6	73.1	44.9	77.2
Second resonance f_2 (kHz), air	205	121	575	308	477
Second resonance f_2 (kHz), water	81.6	43.5	218	126	178

TABLE II. Material properties required for the theoretical predictions.

Parameter	Material	Value
Density ρ_f (kg/m^3)	Air	1.21
Density ρ_f (kg/m^3)	Water	998
Density ρ_c (kg/m^3)	Silicon	2300
Viscosity μ (kg/m s)	Air	1.98×10^{-5}
Viscosity μ (kg/m s)	Water	1×10^{-3}

a tip mass changes the shape of the second eigenmode compared to the second eigenmode of an ideal tipless microcantilever.

(5) In water, the second ODS of all the microcantilevers (A–D) is similar. This surprising result implies that in water, the presence or absence of tip mass does not significantly affect the second eigenmode shape. This result is clearly contrary to the result in air.

We now consider the implications of these measurements for the equivalent stiffnesses and optical lever sensitivities of the second eigenmode in air and water for the different microcantilevers.

C. Experimental results: Equivalent stiffnesses of eigenmodes in air versus water

We wish to calculate the equivalent stiffness for each eigenmode of these microcantilevers. However, as pointed out above, we do not measure directly the eigenmodes but rather the ODSs so the eigenmodes must be extracted from the ODSs. The eigenmode shape equation will be derived in Sec. III. For now we simply state that the general eigenmode shape for a cantilever beam as a function of the axial position x nondimensionalized by the microcantilever length is

$$\Phi_i(x) = \Phi(x,\alpha_i) = \sin(\alpha_i x) - \sinh(\alpha_i x) - \frac{\sin\alpha_i + \sinh\alpha_i}{\cos\alpha_i + \cosh\alpha_i}[\cos(\alpha_i x) - \cosh(\alpha_i x)], \quad (1)$$

where $i=1,2$ represent the first and second eigenmodes, and the eigenmodes are normalized such that $\Phi_i(1)=1$.[11] The first ODS is expected to contain only the first eigenmode. Thus the value α_1 is fitted so that $\Phi_1(x)$ matches the first ODS (in a least squared sense). However, in liquids, the second ODS contains contributions from the first and second eigenmodes due to the low quality factors and this is accounted for in extracting Φ_2.[28]

Once the eigenmodes have been extracted, the equivalent stiffness of each eigenmode is computed from[11]

$$k_i = \frac{EI}{L^3}\int_0^1 [\Phi_i''(x)]^2 dx, \quad (2)$$

where x, E, and I are the distance from the clamp along the microcantilever axis scaled by the microcantilever length, Young's modulus, and cross sectional area moment, respectively, and $(\cdot)'$ denotes x-differentiation. It should be emphasized that equivalent stiffnesses are dependent on the choice of normalization, and requiring $\Phi_i(1)=1$ is a useful choice for AFM applications. That is, the equivalent point-mass model is chosen such that the deflection of the point mass is equal to the deflection at the free end of the microcantilever.[11]

In practice, Eq. (2) is difficult to apply directly. The value of I may not be known because it depends on the microcantilever thickness, which is difficult to measure. Indeed, one reason for the popularity of Sader's[4] method for experimental stiffness calibration over previous methods is that it does not depend on measuring the microcantilever thickness. To avoid this difficulty, this paper will focus on stiffness ratios, either the ratio of equivalent stiffness in air versus water or the ratio of equivalent stiffness to static bending stiffness k_c. This obviates the need to know I or E.

The measured equivalent stiffnesses of the second ODSs of the cantilevers in air and water are listed in Table III, from which three observations can be made.

(1) Microcantilevers C and D have a significantly lower k_2 in water as compared to air, while for microcantilevers A and B the ratio $k_2^{\text{water}}/k_2^{\text{air}}$ is near unity.
(2) Microcantilever A and B's k_2^{air}/k_c are both within 6% of the theoretical value for a uniform rectangular beam ($k_2/k_c=40.6$, where k_c is the static bending stiffness), while microcantilever C and D's k_2^{air}/k_c are significantly greater than this.
(3) Microcantilevers A–D's k_2^{water}/k_c are all within 15% of each other.

TABLE III. Calculated and fit parameters for the microcantilevers (second bending mode). α_2 is fitted to experimental data; all other parameters are calculated.

Microcantilever		A		B		C		D		E	
Condition		Air	Water	Air	Water	Air	Water	Air	Water	Air	Water
Added fluid mass (g) [Eq. (6)]	$M(\omega)$	4.87×10^{-13}	2.85×10^{-10}	1.75×10^{-10}	9.91×10^{-8}	2.21×10^{-10}	1.46×10^{-7}	4.40×10^{-10}	2.93×10^{-7}	2.00×10^{-10}	1.32×10^{-7}
$\frac{\text{Fluid mass}}{\text{Microcantilever mass}}$ [Eq. (12)]	γ	0.049	28.46	0.024	13.5	0.020	14.0	0.011	7.28	0.006	4.27
Dispersion [see Eq. (1)]	α_2	4.66	4.74	4.74	4.80	4.45	4.89	4.51	4.81	4.94	5.15
$\frac{\text{Tip mass}}{\text{Effective microcantilever mass}}$ [Eq. (13)]	$\bar{m}_2$	0	0	≈0	≈0	0.212	0.014	0.059	0.007	0	0
Equivalent stiffness [Eq. (2)]	k_2/k_c	42.5	38.1	38.1	35.5	64.9	32.7	56.1	35.2	31.5	28.7
Stiffness ratio	$\frac{k_2^{\text{water}}}{k_2^{\text{air}}}$	**0.90**		**0.93**		**0.50**		**0.63**		**0.91**	
Optical lever sensitivity [Eq. (3)]	χ_2	4.92	4.62	4.61	4.41	6.08	4.15	5.67	4.38	4.01	3.51
Optical lever sensitivity ratio	$\frac{\chi_2^{\text{water}}}{\chi_2^{\text{air}}}$	**0.94**		**0.96**		**0.68**		**0.77**		**0.88**	

D. Experimental results: Optical lever sensitivities

Most AFMs do not measure the deflection of the microcantilever directly, but instead measure the slope of the microcantilever at the free end. The slope is converted to an equivalent deflection by way of an experimental calibration factor, which is referred to as the optical lever sensitivity. Because each eigenmode has a different slope at the free end, each eigenmode must have a different optical lever sensitivity.[6,8]

Using the same fit to experimental data as described above, the optical lever sensitivity χ_i of the extracted ith eigenmode is calculated as

$$\chi_i = \frac{\partial}{\partial x}\Phi_i(1). \tag{3}$$

The results are listed in Table III. For microcantilevers A and B, χ_2^{air} and χ_2^{water} are close to each other, while those of microcantilevers C and D are significantly smaller (37% and 30%, respectively) in water than in air.

E. Experimental summary

The experimental results clearly show that (1) for cantilevers A and B (tipless or with negligible tip mass), the second eigenmode stiffness and optical lever sensitivity are similar in air or water and (2) for cantilevers C and D (with tip mass), the second eigenmode stiffness and the optical lever sensitivity decrease significantly when the microcantilevers are immersed in water.

III. THEORY

To provide a physical explanation for these results, the eigenmode shapes of a hydrodynamically loaded microcantilever with a tip mass are investigated analytically. There have been a number of recent papers considering hydrodynamic loading and its implications for AFM (e.g., Refs. 5 and 29–33). Most of these papers have focused on effects on resonance frequency and quality factor rather than the eigenmode shapes, stiffnesses, and optical lever sensitivities that are considered here. A few works[23] have investigated the effects on eigenmode shapes, but the effects and their implications for AFM calibration were not fully explored. The effect of tip mass on the eigenmode shapes in air has been reported previously,[34,35] but the focus was mainly on optical lever sensitivity and static bending stiffness and the effects in liquids were not explored. One key idea—that tipped and tipless microcantilever eigenmodes would be similar in water due to dominance of hydrodynamic added mass—was suggested in Ref. 36. Their discussion was framed in terms of resonant frequencies and quality factors.

The hydrodynamic loading is typically described by its Fourier transform.[23,37] The nondimensional equation of motion for the transverse vibrations of a long slender microcantilever with uniform cross section subject to a hydrodynamic force in an incompressible, viscous fluid is given by

$$\frac{EI}{L^3}\hat{w}''''(x,\omega) - \omega^2\rho_c AL\hat{w}(x,\omega) = \frac{\pi}{4}\rho_f\omega^2 b^2\Gamma(\omega)\hat{w}(x,\omega)L, \tag{4}$$

where x, w, ω, ρ_c, A, ρ_f, b, L, and Γ are the coordinate along the microcantilever nondimensionalized by the length, transverse deflection, frequency, microcantilever density, microcantilever cross sectional area, fluid density, microcantilever width, microcantilever length, and hydrodynamic function,[38] respectively, $\hat{(\cdot)}$ denotes the Fourier transform, and $(\cdot)'$ denotes x-differentiation. The hydrodynamic function is complex valued with the real part representing the fluid inertial forces and the imaginary part representing the fluid viscous forces. The boundary conditions are

$$\hat{w}(0,\omega) = 0, \quad \hat{w}'(0,\omega) = 0, \quad \hat{w}''(1,\omega) = 0,$$
$$\frac{EI}{L^3}\hat{w}'''(1,\omega) = -m_{\text{tip}}\omega^2\hat{w}(1,\omega), \tag{5}$$

where m_{tip} is the tip mass. The hydrodynamic force can be written in terms of separate added mass $[\hat{M}(\omega)]$ and viscosity $[\hat{c}(\omega)]$ coefficients:

$$\hat{M}(\omega) = \frac{\pi}{4}\rho_f b^2\,\text{Re}[\Gamma(\omega)]L,$$

$$\hat{c}(\omega) = -\frac{\pi}{4}\rho_f\omega b^2\,\text{Im}[\Gamma(\omega)]L. \tag{6}$$

It can be shown that the viscous damping has little effect on the eigenmode shapes so that the term is neglected and Eq. (4) is written as

$$\frac{EI}{L^3}\hat{w}''''(x,\omega) - \omega^2[\rho_c AL + \hat{M}(\omega)]\hat{w}(x,\omega) = 0. \tag{7}$$

To solve the eigenvalue problem (7), a standard separation of variables $\hat{w}(x,\omega) = W(x)e^{i\omega t}$ yields

$$W''''(x) - \alpha^4 W(x) = 0, \tag{8}$$

$$\frac{L^3}{EI}\omega^2[\rho_c AL + \hat{M}(\omega)] = \alpha^4. \tag{9}$$

The general solution for W in Eq. (8) is

$$\Phi_i(x) = C_1\sin(\alpha_i x) + C_2\sinh(\alpha_i x) + C_3\cos(\alpha_i x) + C_4\cosh(\alpha_i x). \tag{10}$$

Substituting Eq. (10) into Eq. (5) and setting the determinant to zero yield the following characteristic equation:

$$m_{\text{tip}}\omega^2[\sinh(\alpha)\cos(\alpha) - \sin(\alpha)\cosh(\alpha)] + \frac{EI}{L^3}\cos(\alpha)\cosh(\alpha)\alpha^3 + \frac{EI}{L^3}\alpha^3 = 0, \tag{11}$$

which must hold for Eq. (10) to have a nontrivial solution. Solving for the coefficients C_i yields that nontrivial solution, namely, the cantilever mode shape equation (1).

Defining

$$\gamma_n(\omega) = \frac{\hat{M}(\omega)}{\rho_c AL} \tag{12}$$

as the nondimensional ratio of added fluid mass to microcantilever mass in the nth eigenmode and

$$\bar{m}_n(\omega) = \frac{m_{\text{tip}}}{\rho_c AL[1+\gamma_n(\omega)]} \tag{13}$$

as the nondimensional ratio of the tip mass to the remainder of the mass (microcantilever mass plus added fluid mass), Eq. (11) can be written in the form

$$\cos\alpha_n \cosh\alpha_n + 1 + \bar{m}_n(\omega)\alpha_n(\cos\alpha_n \sinh\alpha_n - \sin\alpha_n \cosh\alpha_n) = 0. \tag{14}$$

In the case that $m_{\text{tip}}=0$, then ω does not appear in Eq. (11), and the solutions for α are the same as those for a beam with no hydrodynamic loading. Consequently from Eq. (1), the eigenmodes are the same as those for a beam with no hydrodynamic loading. But if $m_{\text{tip}} \neq 0$ then Eqs. (9) and (14) form two coupled equations in the two unknowns α and ω that link the wavelength α of a flexural wave to its natural frequency ω. In this case α, and thus the eigenmode shape, depends on the added hydrodynamic mass $\hat{M}(\omega)$. In what follows we investigate this case in more detail.

A. Tipped versus tipless microcantilever in a fluid

Our goal here is to derive formulas that can be used to estimate the change in eigenmode shapes, stiffnesses, and optical lever sensitivity when a small tip mass is added to an otherwise uniform rectangular beam in a fluid. That is, we want to know the dependence of k_n and χ_n on $\bar{m}_n$.

The determination of $\bar{m}_n$ could be done in one of three ways.

(1) In an experiment, one can measure the resonant frequency either from a driven tuning curve or from a thermal noise spectrum. From the measured resonant frequency, one can use an expression for the hydrodynamic function from the literature (e.g., Ref. 23) to calculate $\hat{M}(\omega)$. From this and the known microcantilever geometry and tip mass, $\bar{m}_n$ is calculated from Eqs. (12) and (13).
(2) As with calculation of stiffness, one problem with the above method is that the microcantilever thickness may not be well known, so there may be some uncertainty in the direct calculation of microcantilever mass. Experimentalists who wish to reduce the uncertainty in mass may wish to either use a standard stiffness calibration method to determine an estimate for thickness or use a standard stiffness calibration method combined with a measurement of the natural frequency to determine a modal mass directly.
(3) For an analytical calculation, the situation is more complicated because ω and α are coupled. However, one could guess a value for ω, calculate $\hat{M}(\omega)$ and then $\bar{m}_n$, solve for α from Eq. (14), and then calculate a new value for ω from Eq. (9). This procedure can be iterated until $\bar{m}_n$ converges to a fixed value.

Once $\bar{m}_n$ is known, one can work with Eq. (14) exclusively and can disregard Eq. (9). Equation (14) can be solved for α_n numerically and then Eq. (2) can be used to calculate the equivalent stiffness of the eigenmode. To make the dependence of stiffness on $\bar{m}_n$ clear, α and stiffness values are calculated numerically at different values of $\bar{m}_n$ and then a polynomial is fitted by least squares. This leads to the following simple expressions that link the equivalent stiffness of the first, second, and third eigenmodes (k_1, k_2, and k_3) to the $\bar{m}_n$, the ratio of tip mass to the total mass (microcantilever+hydrodynamic mass of the nth eigenmode), and k_c the static bending stiffness of the microcantilever:

$$k_1(\bar{m}_1) \approx k_c(1.03 - 0.181\bar{m}_1 - 0.470\bar{m}_1^2 - 0.431\bar{m}_1^3),$$

$$k_2(\bar{m}_2) \approx k_c(40.3 + 278\bar{m}_2 + 692\bar{m}_2^2 - 44.5\bar{m}_2^3),$$

$$k_3(\bar{m}_3) \approx k_c(315 + 4234\bar{m}_3 + 21\,230\bar{m}_3^2 - 500\bar{m}_3^3). \tag{15}$$

The curve fits have less than 0.6% error over the range $0 < \bar{m}_n < 0.5$. When $m_{\text{tip}}=0$, then $\bar{m}_1=\bar{m}_2=\bar{m}_3=0$, and we recover the standard result for a tipless uniform rectangular microcantilever in a fluid. It is clear from these expressions that the first eigenmode stiffness is quite insensitive to the nondimensional tip mass but the second and higher-order eigenmode stiffnesses are sensitive to the nondimensional tip mass. This explains why the first eigenmode is similar in all of the experimental cases (air or water) but the second eigenmode is not.

Using this curve fit we now quantitatively explain the observed experimental results for all the microcantilevers (reference parameters in Tables I–III). Microcantilever C has a large tip such that $m_{\text{tip}}/\rho_c AL$ is approximately 0.22 (estimate based on dimensions from scanning electron microscopy images). In air, γ is small, $\bar{m}_2^{\text{air}}=m_{\text{tip}}/(1+\gamma)=0.22/(1+0.021)=0.212$; thus the second eigenmode is stiffened in air: $k_2^{\text{air}} \approx 130k_c$. However, in water γ is large (the added fluid mass is 14 times larger than the mass of the microcantilever itself) and this added fluid mass dilutes the effect of the tip mass such that $\bar{m}_2^{\text{water}}=0.22/(1+14)=0.014$. Thus the second eigenmode is only slightly stiffened in water: $k_2^{\text{water}} \approx 44.4k_c$, which is close to what is expected for a uniform tipless microcantilever. The theory predicts that the ratio of $k_2^{\text{water}}:k_2^{\text{air}}$ is 0.34:1 compared to the experimental value of 0.5:1 in Sec. II B. For microcantilever D, the theory predicts $k_2^{\text{water}}:k_2^{\text{air}}=0.72:1$ compared to the experimental value of 0.63:1. Thus the theoretical expressions are reasonably close to experimental measurements.

In contrast, microcantilever A has no tip such that $\bar{m}_n$ is zero in both air and water and microcantilever B has a hollow tip such that $|\bar{m}_n| \ll 1$ in both air and water. Thus, the first and second eigenmodes of microcantilevers A and B are expected to be similar in both air and water. This is borne out by the experimental data presented in Fig. 2 and Table III. The theory would predict $k_2^{\text{water}}:k_2^{\text{air}}$ to be exactly 1:1 for both microcantilevers. In fact, $k_2^{\text{water}}:k_2^{\text{air}}$ is 0.90:1 for microcantilever A and 0.93:1 for microcantilever B, slightly lower than predicted. This small deviation from the prediction is likely

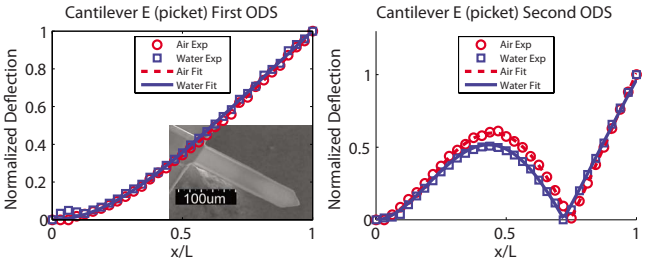

FIG. 3. (Color online) Measured ODSs for picket shaped microcantilever E in air and water. Left column first ODS (first eigenmode) and right column second ODS (first eigenmode plus second eigenmode).

due to three-dimensional hydrodynamic effects at the free end of the microcantilever that the preceding two-dimensional theory cannot account for.

Now, following the same fitting procedure but for optical lever sensitivity (3) instead of stiffness, it is possible to derive simple expressions for χ_i, the optical lever sensitivity of a uniform rectangular microcantilever immersed in a fluid in terms of the nondimensional tip mass $\bar{m}_n$ (tip mass divided by the sum of microcantilever mass and hydrodynamic mass of nth eigenmode),

$$\chi_1(\bar{m}_1) \approx 1.38 + 0.315\bar{m}_1 - 0.331\bar{m}_1^2,$$

$$\chi_2(\bar{m}_2) \approx 4.81 + 16.8\bar{m}_2 - 0.766\bar{m}_2^2,$$

$$\chi_3(\bar{m}_3) \approx 7.91 + 50.7\bar{m}_3 - 1.15\bar{m}_3^2. \quad (16)$$

As with equivalent stiffness, the first eigenmode optical lever sensitivity does not change significantly with $\bar{m}_n$ while the second and higher eigenmode sensitivity increases significantly with $\bar{m}_n$. Because $\bar{m}_n$ is small in water compared to air (due to large density of water) we expect the optical lever sensitivity for a tipped microcantilever to be lower in water than in air. This is clearly observed in the measurements as tabulated in Table III where the optical lever sensitivity of the second eigenmodes of microcantilevers C and D decreases by nearly 20%–30% when placed in water.

To summarize, the nondimensional ratio $\bar{m}_n$ is the key parameter in this analysis. When $\bar{m}_n$ is large (large tip mass and/or small hydrodynamic added mass) then the higher-order eigenmodes, equivalent stiffnesses, and optical lever sensitivities are affected by the tip. When $\bar{m}_n$ is small (small tip mass and/or large hydrodynamic added mass) then the higher-order eigenmodes, equivalent stiffnesses, and optical lever sensitivities are not affected by the tip and the microcantilever behaves as if it were tipless. This result is consistent with a suggestion in Ref. 36 and complements the large body of previous work on the effects of tip mass and hydrodynamic loading on the resonant frequencies and quality factors of microcantilevers in liquids.

IV. PICKET CANTILEVERS

Thus far only microcantilevers of constant section have been studied, whereas microcantilever E has a picket shaped end (but it is tipless). The measured ODSs of microcantilever E are shown in Fig. 3. Comparing Fig. 3 to the previous microcantilevers in Fig. 2, the following conclusions are clearly drawn.

(1) The first eigenmode of picket shaped tipless microcantilevers is nearly unaffected when placed in water from air.
(2) The second eigenmode of the picket shaped microcantilever E is changed slightly when placed in water from air.
(3) The second eigenmode of microcantilever E in air is different from those of the tipless microcantilevers A and B.

Using the same fitting procedure as in Sec. II C, α_i, k_i, and χ_i are extracted from the experimental data for microcantilever E, and the results are shown in Table III. $k_2^{\text{water}}/k_2^{\text{air}}$ is 0.91, similar to that of microcantilever A. $\chi_2^{\text{water}}/\chi_2^{\text{air}}$ is 0.88, slightly lower than that of microcantilever A. But, microcantilever E's k_2^{air}/k_c is 25% softer than that of microcantilever A. How are these results to be explained?

A picket shaped microcantilever can be considered a rectangular microcantilever with some material removed from near the free end. Thus a picket shaped microcantilever can be modeled as a uniform rectangular microcantilever with a *negative* tip mass. Since a positive tip mass stiffens the higher-order eigenmodes and increases the optical lever sensitivity in air, negative tip mass should soften higher-order eigenmodes and decrease the optical lever sensitivity in air,[11] which is consistent with the observations in the preceding paragraph.

However, the negative tip mass analogy breaks down in water. Contrary to the behavior of the microcantilever with tip mass, microcantilever E's second eigenmode does not become more like microcantilever A's second eigenmode when it is immersed in water. The reasons for this cannot be fully explained. However, the preceding theory was developed for uniform beams (two-dimensional fluid flow), whereas a picket shaped microcantilever may have a three-dimensional fluid flow near the free end.

V. DISCUSSION AND IMPLICATIONS FOR DYNAMIC AFM

Considering the above results, it is clear that for microcantilevers with any significant tip mass, it is preferable to calibrate the higher-order eigenmode stiffnesses and optical lever sensitivities directly in the desired imaging media, rather than calibrating in air and then using that value for operating in liquid. Of course, based on the results of Refs. 2 and 20, there may be more uncertainty in a stiffness calibration in liquid than there is in air. But given the magnitude of the difference in stiffness between air and water, some uncertainty in a correct stiffness may be preferable to absolute certainty in an incorrect stiffness.

The results presented in this work are useful in a number of contexts where accurate knowledge of higher-order eigenmode stiffness is important.

(1) In bimodal AM-AFM,[39] two eigenmodes are excited simultaneously. A goal of bimodal AFM is to provide information on sample material properties such as elastic-

ity and dissipation by using the second eigenmode as an additional signal channel. For example, the phase of the second eigenmode has been shown to be significantly more sensitive to material properties than the phase of the first eigenmode.[40] The quantitative interpretation of bimodal AFM (i.e., relating observables such as phase shift to tip-sample dissipation) depends on accurate knowledge of the stiffness of the higher-order eigenmodes.[13,14]

(2) Even for situations where only a single eigenmode is excited, it may be preferable to excite an eigenmode other than the fundamental. Several groups have shown that operating AFM in higher eigenmodes can give superior phase contrast images in tapping mode as compared to the first eigenmode[41,42] and enables very small oscillation amplitudes in frequency modulation (FM)-AFM comparable to the decay length of the interaction forces, and thus increases the lateral resolution of the images.[43,44] Again, relating the experimental observables to sample properties such as dissipation requires knowledge of the eigenmode stiffness (e.g., Ref. 45).

(3) There is an increasing interest in using FM techniques in liquid environments (e.g., Refs. 46 and 47). Exciting higher eigenmodes may be desirable in FM-AFM in liquids because higher eigenmodes have higher quality factors and stiffnesses than the first eigenmode. FM-AFM allows the entire tip-sample interaction potential to be reconstructed[48] but again this requires accurate knowledge of the eigenmode stiffness.

(4) In low Q environments (liquids), even for situations where only the first eigenmode is directly excited, the tip-sample interaction force may momentarily excite higher eigenmodes.[49] This implies that most AFM operation in liquid is inherently bimodal, and thus higher eigenmodes must be accounted for in order to accurately model the dynamics. For example, the momentarily excited eigenmodes can give rise to "drum-roll-like" effects in which the tip and sample interact multiple times during one drive cycle.[50] Simulations using the VEDA software[51] show that the bifurcation point between single and double tapping is highly sensitive to the stiffness of the second eigenmode. For example, differences on the order of those observed for microcantilever C in this work (50% difference in k_2) makes the difference between the bifurcation point being at 40% setpoint ratio and 75% setpoint ratio.

VI. CONCLUSIONS

To summarize, the effect of hydrodynamic loading and tip mass on the eigenmode shapes, stiffnesses, and optical lever sensitivities of diving board microcantilevers in air and water has been studied experimentally and analytically. Tipless microcantilevers have similar eigenmode shapes, stiffnesses, and optical lever sensitivities in both air and water. The nondimensional ratio $\bar{m}_n$ has been identified as the key parameter that determines the effect of tip mass on the overall inertial loading of the microcantilever. A tip mass of more than a few percent of the total microcantilever mass stiffens the second and higher-order eigenmodes and increases their optical lever sensitivities in air. But in water, the effect of tip mass is diluted by the large hydrodynamic loading. Because hydrodynamic inertia is large in liquid, the tip mass effect is negligible compared to the large hydrodynamic mass. Thus the second and higher-order eigenmodes of tipped microcantilevers are softer in water than in air. A picket shape softens the second and higher-order eigenmodes in air but this effect is not diluted in liquid. Therefore, for any microcantilever except a tipless rectangular microcantilever, a calibration of higher eigenmodes taken in air may not be directly usable in liquid.

ACKNOWLEDGMENTS

This research was funded in part by the National Science Foundation through Grant No. CMMI-0700289. The authors also thank Professor Ron Reifenberger (Physics Department, Purdue), John Melcher (Mechanical Engineering, Purdue), and José R. Lozano (Instituto de Microelectrónica de Madrid) for valuable discussions and comments on an early version of this manuscript.

[1] N. A. Burnham, X. Chen, C. S. Hodges, G. A. Matei, E. J. Thoreson, C. J.Roberts, M. C. Davies, and S. J. B. Tendler, Nanotechnology **14**, 1 (2003).
[2] D. G. Cole, Meas. Sci. Technol. **19**, 125101 (2008).
[3] C. P. Green, H. Hadi, J. P. Cleveland, R. Proksch, P. Mulvaney, and J. E. Sader, Rev. Sci. Instrum. **75**, 1998 (2004).
[4] J. E. Sader, J. W. M. Chon, and P. Mulvaney, Rev. Sci. Instrum. **70**, 3967 (1999).
[5] F.-J. Elmer and M. Dreier, J. Appl. Phys. **81**, 7709 (1997).
[6] T. E. Schäffer, Nanotechnology **16**, 664 (2005).
[7] R. W. Stark, Rev. Sci. Instrum. **71**, 5053 (2004).
[8] T. E. Schäffer and H. Fuchs, J. Appl. Phys. **97**, 083524 (2005).
[9] G. Binnig, C. F. Quate, and C. Gerber, Phys. Rev. Lett. **56**, 930 (1986).
[10] H.-J. Butt, B. Cappella, and M. Kappl, Surf. Sci. Rep. **59**, 1 (2005).
[11] J. Melcher, S. Hu, and A. Raman, Appl. Phys. Lett. **91**, 053101 (2007).
[12] R. Proksch, T. E. Schäffer, J. P. Cleveland, R. C. Callahan, and M. B. Viani, Nanotechnology **15**, 1344 (2004).
[13] J. R. Lozano and R. García, Phys. Rev. Lett. **100**, 076102 (2008).
[14] J. R. Lozano and R. García, Phys. Rev. B **79**, 014110 (2009).
[15] N. F. Martínez, J. R. Lozano, E. T. Herruzo, F. Garcia, C. Richter, T. Sulzbach, and R. Garcia, Nanotechnology **19**, 384011 (2008).
[16] M. K. Abak, O. Aktas, R. Mammadov, İ. Gürsel, and A. Dâna, Appl. Phys. Lett. **92**, 223113 (2008).
[17] O. Sahin, C. F. Quate, O. Solgaard, and A. Atalar, Phys. Rev. B **69**, 165416 (2004).
[18] X. Xu, J. Melcher, S. Basak, R. Reifenberger, and A. Raman, Phys. Rev. Lett. **102**, 060801 (2009).
[19] A. Raman, J. Melcher, and R. Tung, Nanotoday **3**, 20 (2008).
[20] T. Pirzer and T. Hugel, Rev. Sci. Instrum. **80**, 035110 (2009).
[21] The cantilevers were completely immersed in water several millimeters from any wall; thus squeeze film effects are negligible.
[22] D. J. Ewins, *Modal Testing: Theory, Practice and Application*, 2nd ed. (Research Studies Press, Ltd., Hertfordshire, UK, 2000).
[23] J. E. Sader, J. Appl. Phys. **84**, 64 (1998).
[24] http://probe.olympus-global.com.
[25] www.agilent.com.
[26] www.spmtips.com.
[27] www.appnano.com.
[28] The lsqcurvefit command in MATLAB was used for the curve fitting. The first ODS was fitted to the function $C_1\Phi(x,\alpha_1)$ by choosing values of α_1 and C_1, where C_1 is an arbitrary scaling constant. The second ODS was fitted to the function $C_1\Phi(x,\alpha_1)+C_2\Phi(x,\alpha_2)$ by considering α_1 to be fixed and equal to the value from the first ODS fit and choosing values of C_1, C_2, and α_2.
[29] S. Basak, A. Raman, and S. Garimella, J. Appl. Phys. **99**, 114906 (2006).
[30] C. Rankl, V. Pasushenko, F. Kienberger, C. Stroh, and P. Hinterdorfer,

Ultramicroscopy **100**, 301 (2004).
[31]C. A. V. Eysden and J. E. Sader, J. Appl. Phys. **101**, 044908 (2007).
[32]M. K. Ghatkesar, T. Braun, V. Barwich, J.-P. Ramseyer, C. Gerber, M. Hegner, and H. P. Lang, Appl. Phys. Lett. **92**, 043106 (2008).
[33]R. C. Tung, A. Jana, and A. Raman, J. Appl. Phys. **104**, 114905 (2008).
[34]M. S. Allen, H. Sumali, and P. C. Penegor, 27th International Modal Analysis Conference, 2009 (unpublished).
[35]M. S. Allen, H. Sumali, and P. C. Penegor, J. Dyn. Syst., Meas., Control **131**, 064501 (2009).
[36]J. W. M. Chon, P. Mulvaney, and J. E. Sader, J. Appl. Phys. **87**, 3978 (2000).
[37]E. O. Tuck, J. Eng. Math. **3**, 29 (1969).
[38]Note that $\Gamma(\omega)$ is assumed to have no x dependence. This may not be valid if the microcantilever is close to and inclined with respect to the substrate (Ref. 52).
[39]T. R. Rodríguez and R. García, Appl. Phys. Lett. **84**, 449 (2004).
[40]N. F. Martínez, S. Patil, J. R. Lozano, and R. García, Appl. Phys. Lett. **89**, 153115 (2006).
[41]A. Ulcinas and V. Snitka, Ultramicroscopy **86**, 217 (2001).
[42]R. W. Stark, T. Drobek, and W. Heckl, Appl. Phys. Lett. **74**, 3296 (1999).
[43]Y. Sugimoto, S. Innami, M. Abe, Ó. Custance, and S. Morita, Appl. Phys. Lett. **91**, 093120 (2007).
[44]S. Kawai and H. Kawakatsu, Appl. Phys. Lett. **88**, 133103 (2006).
[45]B. Anczykowski, B. Gotsmann, H. Fuchs, J. P. Cleveland, and V. B. Elings, Appl. Surf. Sci. **140**, 376 (1999).
[46]M. J. Higgins, C. K. Riener, T. Uchihashi, J. E. Sader, R. McKendry, and S. P. Jarvis, Nanotechnology **16**, S85 (2005).
[47]T. Fukuma, A. Mostaert, L. Serpell, and S. Jarvis, Nanotechnology **19**, 384010 (2008).
[48]J. E. Sader and S. P. Jarvis, Appl. Phys. Lett. **84**, 1801 (2004).
[49]S. Basak and A. Raman, Appl. Phys. Lett. **91**, 064107 (2007).
[50]J. Melcher, X. Xu, and A. Raman, Appl. Phys. Lett. **93**, 093111 (2008).
[51]J. Melcher, S. Hu, and A. Raman, Rev. Sci. Instrum. **79**, 061301 (2008).
[52]R. Tung, "Hydrodynamic damping of microcantilevers near solid walls," MS thesis, Purdue University, 2008.